Exotic surface magnetotransport phenomena in the antiferromagnetic Mott insulator NiS_2

Sami El-Khatib,[1,2,3,*] Faisal Mustafa,[2] Mehmet Egilmez,[1,2] Bhaskar Das,[3] Yu Tao,[3] Moumita Maiti,[3] Yeon Lee,[3] and Chris Leighton[3,†]

[1]*Department of Physics, American University of Sharjah, Sharjah PO Box 26666, United Arab Emirates*
[2]*Materials Science and Engineering Program, American University of Sharjah, Sharjah PO Box 26666, United Arab Emirates*
[3]*Department of Chemical Engineering and Materials Science, University of Minnesota, Minneapolis, Minnesota 55455, USA*

(Received 15 July 2023; accepted 26 September 2023; published 10 October 2023)

The pyrite-structure transition-metal disulfide NiS_2 is in principle a model cubic antiferromagnetic Mott insulator that can be doped through insulator-metal transitions with both electrons and holes (in $Ni_{1-x}Cu_xS_2$ and $Ni_{1-x}Co_xS_2$), eventually inducing superconductivity and ferromagnetism, respectively. Magnetism and transport have proven challenging to understand in NiS_2, however. The antiferromagnetic spin structure below ~39 K is complex due to frustration, while unexplained weak ferromagnetism emerges below ~30 K. Surface conduction is also now understood to dominate in NiS_2 at low temperatures, raising questions about the interpretation of decades of prior data. Here, we present a complete study of the surface magnetotransport phenomena that emerge at low temperatures in high-quality single-crystal NiS_2, which turn out to be strikingly rich. On cooling, isotropic magnetoresistance due to a field-induced shift of the first-order weak ferromagnetic ordering transition is first uncovered, i.e., metamagnetic magnetoresistance. At lower temperatures, larger, anisotropic magnetoresistance effects arise due to distinct switching events associated with the weak ferromagnetism. Strong evidence is presented that this is due to a field-driven in-plane to out-of-plane reorientation of surface spins, likely correlated with surface steps and terraces. In-plane exchange bias accompanies these effects, further supporting this interpretation. At the lowest temperatures, the spin reorientation field eventually exceeds the 9-T measurement window, generating strongly field-asymmetric magnetoresistance. Some of these unusual phenomena also manifest in the Hall channel, culminating in a sizable anomalous Hall effect at low temperatures. These results significantly demystify recent magnetoresistance and magnetic microscopy observations in NiS_2 crystals and nanoflakes, and constitute an important step in elucidating the complex electronic and magnetic properties of this pivotal antiferromagnetic Mott insulator.

DOI: 10.1103/PhysRevMaterials.7.104401

I. INTRODUCTION

Mott insulators, and the insulator-metal transitions (IMTs) they display versus doping and bandwidth, hold a particularly important place in condensed matter and materials physics, and have been intensively studied in many materials (e.g., [1–3]). The pyrite-structure transition-metal (TM) disulfide NiS_2 is one such material [4–15], which is of particular interest due to its relatively simple, cubic structure, and the band-filling-controlled evolution of the electronic and magnetic ground states in TMS_2 pyrites [4–7]. Specifically, pyrite-structure FeS_2, CoS_2, NiS_2, and CuS_2 have $t_{2g}^6e_g^0$, $t_{2g}^6e_g^1$, $t_{2g}^6e_g^2$, and $t_{2g}^6e_g^3$ electronic configurations, respectively, leading to diamagnetic semiconducting, ferromagnetic (F) metallic, antiferromagnetic (AF) Mott-insulating, and metallic/superconducting ground states [4–7]. Ternary systems such as $Ni_{1-x}Co_xS_2$ and $Ni_{1-x}Cu_xS_2$ thus enable doping of AF Mott-insulating NiS_2 with both holes and electrons [16–19], while Se substitution (e.g., in $NiS_{2-x}Se_x$) enables bandwidth control [20–24], rendering NiS_2 particularly attractive for the study of the transition from Mott insulator to metal.

Despite this promise as a model system, both magnetic and electronic properties of NiS_2 have proven challenging to understand. NiS_2 orders antiferromagnetically below a Néel temperature, $T_N \approx 39$ K, but with a complex noncollinear spin structure likely related to the geometric frustration inherent to the fcc Ni sublattice [9,11,13,24,25]. This frustration is apparent through a large ratio of the Curie-Weiss temperature to T_N (~30) [11,26], accompanied by indications of short-range ordering and deviations from ideal Curie-Weiss behavior [25,26]. Most intriguingly, weak ferromagnetism (WF) then turns on via a first-order transition at a temperature $T_{wf} \approx 30$ K [9–11,14,19,24–26]. While WF is not uncommon in AFs due to effects such as spin canting, it is nominally forbidden in the pyrite NiS_2 space group [24]. Distortions from the accepted structure have thus been proposed to explain the WF [13,24,25], but with no clear literature consensus, meaning that the WF ground state remains to be fully explained.

Electronic transport in NiS_2 is similarly rich. Insulating behavior with a relatively small transport gap is well established [8,11,13–24,26] but is followed at lower temperature (T) by complex behavior. It is now becoming accepted that this arises because surface conduction is intrinsic to NiS_2 [26–28], as it

*Corresponding author: selkhatib@aus.edu
†Corresponding author: leighton@umn.edu

is to other pyrite TMS_2 compounds such as FeS_2 [29–33]. In essence, likely due to trivial surface states [26], the NiS_2 surface is more conductive than the bulk [26,27]. As NiS_2 single crystals are cooled, freeze-out of the Mott-insulating bulk thus leads to the more conductive surface shunting the current in standard transport measurements, yielding a bulk-to-surface crossover [26]. This surface conduction in NiS_2 was first hypothesized by Thio and Bennett [27] but was recently put on a firmer footing through observation of the above-mentioned T dependence of the resistivity (ρ), successful two-channel (bulk/surface) modeling of transport and magnetotransport, low-T thickness scaling, sensitivity to surface preparation, etc. [26]. The conductive surface layer on NiS_2 single crystals can even be fine-tuned via surface preparation, from a nanoscopic effectively two-dimensional (2D) layer, to an ∼100-nm-thick effectively three-dimensional (3D) weakly localized layer [26].

These recent findings have several implications. First and foremost, the vast majority of the large body of prior work on the electronic properties of NiS_2 across the IMT was performed before these advances [26], meaning that surface conduction was not considered. The extensive work on the IMT in systems such as $NiS_{2-x}Se_x$ [20–24], $Ni_{1-x}Co_xS_2$ [16,17], and $N_{1-x}Cu_xS_2$ [18] thus did not distinguish bulk from surface behavior, meaning that many conclusions are not reflective of the true bulk properties of NiS_2 [26]. Second, the extraordinary recent advances in the understanding of the importance of topology in electronic structure and transport have put a spotlight on surface transport phenomena, increasing the general interest in this area [34–36]. NiS_2 was in fact recently identified as a magnetic material with potentially nontrivial topology [37], although it is far from clear whether this prediction would survive after the inclusion of the strong electronic correlations needed to reproduce the Mott-insulating ground state [38]. Third, given the extensive evidence for surface conduction in FeS_2 [29–33], the importance of surface states in CoS_2 [39], and the now growing evidence for surface states and conduction in NiS_2 [26–28], it becomes plausible that surface conduction is inherent to the entire TMS_2 family [26], generating additional general interest.

Based on the above, further investigation of the electronic and magnetic properties of NiS_2 is clearly warranted. High-quality, thoroughly characterized single crystals are available [8–18,21–23,25–28], with various surface preparations [26], and have been used in detailed studies of temperature- and field-dependent magnetometry [9–11,14,23,25,26], $\rho(T)$ [8,11,12,14–18,21–23,26,27], two-channel (surface/bulk) transport modeling [26], thickness-dependent transport [26], and higher-T magnetoresistance (MR) and Hall effects [26]. What is clearly missing, however, and is likely to be of particular interest given the above, is a detailed study of low-T magnetotransport, particularly below T_N and T_{wf}. AF and WF ordering are known to impact $\rho(T)$ in NiS_2 [14,15,26] but the details of the interplay of AF and WF order with transport are poorly understood, despite that they are likely to be nontrivial and relevant to other materials. A recent study of nanoflakes prepared from NiS_2 single crystals in fact unveiled a remarkable set of phenomena related to the interplay of transport and magnetism [40]. These include pronounced field asymmetry in MR below T_{wf}, exchange-bias effects, and very large low-T MR (*up to 1400%*) with complex magnetic field (H) and T dependence [40]. The latter MR effects were found specifically in local (micron-scale) transport measurements on nanoflake regions with large surface steps [40]. Nitrogen-vacancy-center magnetometry then revealed large uncompensated magnetization at those surface steps, suggesting some interplay between surface conduction and surface WF [40]. Such studies establish complex magnetotransport in surface-dominated NiS_2, with clear interplay with magnetism, but with many unanswered questions regarding mechanisms [40].

Here, we address the above through a comprehensive low-T magnetotransport study of high-quality, thoroughly characterized NiS_2 crystals, deep in the surface-dominated transport regime. Clear anomalies in $\rho(T)$ are detected at T_N and T_{wf}. MR measurements then reveal a sharp negative peak close to T_{wf}, in addition to larger effects at lower T. The effect near T_{wf} is shown to be isotropic MR arising due to the field-driven shift of the first-order transition to WF, i.e., metamagnetic MR, analogous to that seen in other magnetically ordered systems with first-order transitions. At lower T, larger MR effects kick in, with pronounced anisotropy. Specifically, H along [111] (perpendicular to the crystal surface) is shown to induce clear switching events in the WF magnetization and MR, which are absent in in-plane measurements, where exchange bias instead emerges. Considering the prior observation of large uncompensated magnetization at surface step edges [40], we propose a coherent explanation for these phenomena where a field-driven surface spin reorientation transition drives the MR. The critical field for this spin reorientation grows with cooling, eventually exceeding the 9-T measurement window, at which point highly field-asymmetric MR emerges, explaining prior observations [40]. Finally, Hall effect measurements provide complementary observations, including signatures of the spin reorientation transition and a sizable anomalous Hall effect at low T. These findings shed much light on prior observations in NiS_2 nanoflakes [40] and represent an important step toward understanding the electronic and magnetic properties of this pivotal AF Mott insulator.

II. EXPERIMENTAL METHODS

As in recent prior work [26], the NiS_2 single crystals studied here were grown by chemical vapor transport. Details can be found elsewhere [26] but, briefly, precursor powders of Ni (Alfa Aesar, 99.999% purity), S (CERAC, 99.9995% purity), and $NiBr_2$ (Sigma-Aldrich, 99.999% purity) were employed, in evacuated quartz vessels, with hot and cold zone temperatures of 700 °C and 650 °C [26]. Consistent with the crystal habit [see the inset to Fig. 1(e) for an image of a typical crystal] single-crystal x-ray diffraction confirms (111) surface facets [26]. These crystals have been subjected to rigorous prior structural, chemical, magnetic, and electronic characterization, encompassing powder x-ray diffraction, single-crystal x-ray diffraction, x-ray rocking curve analysis, energy-dispersive x-ray spectroscopy, T- and H-dependent magnetometry and (magneto)transport, two-channel transport modeling, etc. [26].

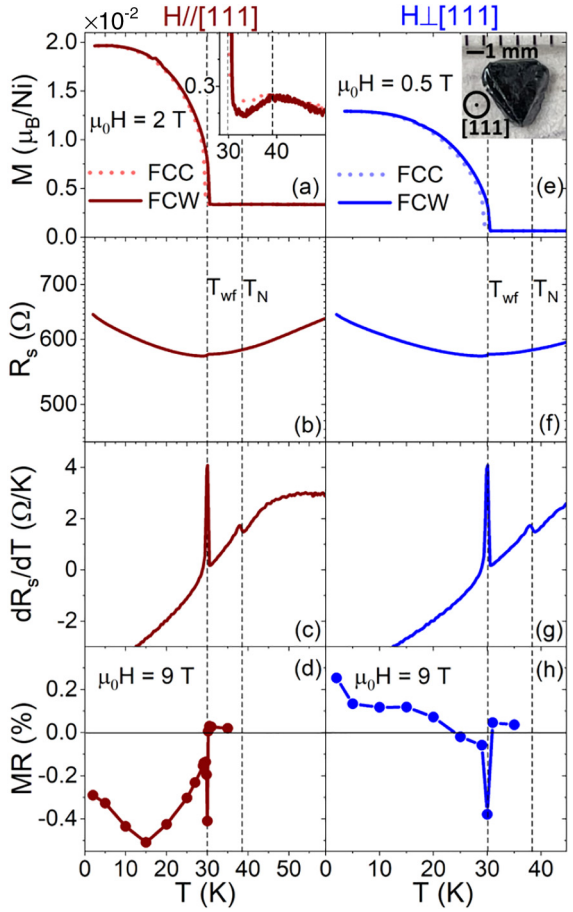

FIG. 1. Temperature (T) dependence of the magnetization M (a),(e), sheet resistance R_s (b),(f), dR_s/dT (c),(g), and percent magnetoresistance MR (d),(h) with the applied magnetic field H parallel to the [111] direction (left panels, red) and perpendicular to the [111] direction (right panels, blue). As shown in the inset to (e), parallel to [111] is out of the crystal plane, while perpendicular to [111] is in the crystal plane. The inset to (a) is a blowup of the region around the Néel temperature. The data in panels (a),(e) are shown for both field-cooled cooling (FCC, dotted lines) and field-cooled warming (FCW, solid lines), in the fields shown. The data in panels (d),(h) are at 9 T. The vertical dashed lines mark the Néel temperature (T_N) and weak ferromagnetic ordering temperature (T_{wf}).

Importantly, the work presented here was performed on double-side-polished crystals. Mechanical polishing is known to enhance surface conduction in NiS_2, resulting in a relatively thick (∼100 nm) surface layer with effectively 3D transport characteristics [26]. This choice of surface preparation was made to ensure that all measurements are deep in the surface-dominated transport regime; the surface-to-bulk crossover occurs at ∼125 K in such crystals [26], while we focus here on <50 K. Six crystals were measured in this study, in addition to ∼12 in prior work [26], and the crystal upon which this paper focuses is representative of all crystals measured of this type. For transport experiments, parallel (111) crystal faces were first polished with SiC paper, followed by 3- and 1-μm diamond slurries. Van der Pauw contacts were then applied using a Micro Point Pro iBond5000 Wedge wire bonder, using Al(99.9%)/Si(1%) wire. Transport and magnetic (vibrating sample magnetometry) measurements were made in a closed-cycle physical property measurement system (Cryogenics Ltd.), from 2 to 310 K in $\mu_0 H$ up to 9 T. All measurements were made with H both parallel to a [111] axis and perpendicular to it, i.e., both out of, and in, the crystal plane, respectively [see the inset to Fig. 1(e)]. Field-dependent magnetization, MR, and Hall effect scans at a given T were recorded by warming above T_N, zero-field cooling to the target T, then sweeping $\mu_0 H$ from 0 to 9 T to −9 T to 9 T. Raw MR/Hall effect data were typically symmetrized/antisymmetrized to correct for contact misalignment effects; these corrections were typically small. As discussed in detail below, however (Sec. III B), at low T, some of the MR effects observed here are highly field asymmetric, and thus were not symmetrized [41].

III. RESULTS AND ANALYSIS

A. Basic magnetic, transport, and magnetotransport characterization

Figures 1(a) and 1(e) first establish that the basic magnetic behavior in the H//[111] and $H\perp$[111] cases is as expected. The moderate-H measurements of the T-dependent magnetization (M) shown in the main panels of Figs. 1(a) and 1(e) are dominated by the onset of WF behavior at $T_{wf} \approx 30$ K [9–11,14,15,25,26]. As can be seen by comparing the field-cooled cooling (FCC, dotted lines) and field-cooled warming (FCW, solid lines) data, weak thermal hysteresis arises, consistent with the first-order WF to AF transition at T_{wf} [10,26]. The second-order AF ordering at T_N is apparent only from closer inspection of $M(T)$ [see the inset to Fig. 1(a)], which reveals the typical peaks at $T_N \approx 39$ K [25,26]. Figures 1(b) and 1(f) then establish typical zero-field sheet resistance (R_s) versus T for polished NiS_2 crystals. The T range here is well below the bulk-to-surface crossover [26], resulting in surface-dominated transport. In polished crystals, R_s falls well below $h/e^2 \approx 26\,k\Omega$, the $R_s(T)$ in Figs. 1(b) and 1(f) (which are identical because $H = 0$) being typical, as quantitatively captured in prior work by weak localization and electron-electron interaction corrections to the $T = 0$ conductance [26]. Also noticeable in Figs. 1(b) and 1(f) is an anomaly in $R_s(T)$ at T_{wf}. This is better illustrated in Figs. 1(c) and 1(g), which plot the T dependence of dR_s/dT, revealing clear anomalies at both T_{wf} and T_N, the former being most prominent, as is typical [14,15,26]. Since this transport is surface dominated, this indicates that both the AF and WF orders in NiS_2 persist to the surface [26], a nontrivial finding. We note as an aside that the observation of an anomaly at T_N in dR_s/dT is at odds with a prior claim that this feature is seen only in flux-grown NiS_2 crystals [14].

With expected behavior in $M(T)$ and $R_s(T)$ established, Figs. 1(d) and 1(h) move on to low-T MR, the primary focus of this paper. Shown are 9-T MR(T) scans for H//[111] and $H\perp$[111], using a red/blue color scheme that is employed in all subsequent figures. As established previously, above T_{wf} there exists a small positive MR of nonmagnetic origin [26]. Of far higher interest in the current context, cooling through T_{wf} leads to a sharp negative peak of approximately −0.4%, independent of the H direction. Below this, slightly larger

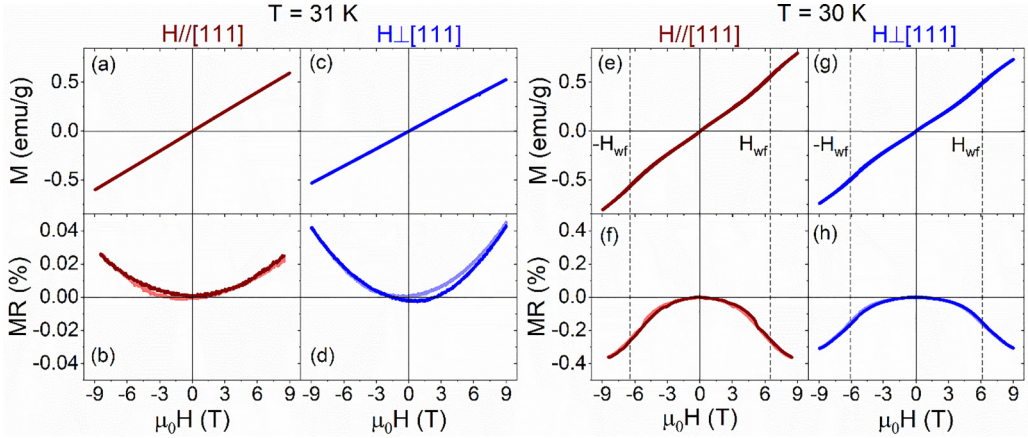

FIG. 2. Applied magnetic field (H) dependence of the magnetization M [top panels (a),(c),(e),(g)] and percent magnetoresistance MR [bottom panels (b),(d),(f),(h)] at temperatures (T) of 31 K [left (a)–(d)] and 30 K [right (e)–(h)]. Data are shown for H parallel to [111] (red) and perpendicular to [111] (blue). At 30 K, the weak ferromagnetic ordering field H_{wf} is marked with the dashed vertical lines.

MR (with magnitude up to >0.5%) is found, in this case with strong anisotropy. The MR with H//[111] is negative and relatively large, while the MR for $H\perp$[111] is positive and smaller. The subsequent sections of this paper seek to explore and understand the MR(T) behavior in these two field directions, breaking it down into the $T \approx T_{wf}$ regime (Sec. III B), the $T < T_{wf}$ regime (Sec. III C), and the lowest-T regime (Sec. III C). As will become clear below, while the MR effects here are modest in these bulk single crystals, it is important to note that they become very large in nanoflakes [40], and therefore likely in films also, which has led to speculation regarding possible applications [40].

B. Magnetoresistance due to field-induced weak ferromagnetism ($T \approx T_{wf}$)

Figure 2 greatly elucidates the origin of the sharp negative MR peak in Figs. 1(d) and 1(h) by examining $M(H)$ and MR(H) in the two H directions just above T_{wf} [at 31 K, Figs. 2(a)–2(d)] and within the narrow hysteresis region around T_{wf} shown in Figs. 1(a) and 1(e) [at 30 K, Figs. 2(e)–2(h)]. At 31 K [Figs. 2(a)–2(d)], things are as expected: $M(H)$ is linear and largely isotropic in the AF phase [Figs. 2(a) and 2(c)], while MR(H) displays somewhat anisotropic parabolic positive MR, similar to prior work at comparable temperatures [26,40]. Cooling into the thermal hysteresis region associated with T_{wf}, however [Figs. 2(e)–2(h)], leads to clear anomalies in $M(H)$ at field magnitudes we denote H_{wf}. At a given T, these fields mark the point at which a field-induced transition from AF to WF phases occurs, i.e., metamagnetism, leading to increased M [10,25,26]. Figures 2(f) and 2(h) reveal that this transition is evident in MR(H) also. The vertical dashed lines in fact mark the points in the $M(H)$ curves at which peaks occur in dM/dH, coinciding with the points at which maxima/minima occur in d(MR)/dH (see Supplemental Material Fig. S1 for more detail [42]). Similar to systems in which first-order AF to F transitions occur as a function of T (e.g., FeRh [43,44]), H-driven transitions from AF to WF can thus be driven in NiS_2 in the vicinity of T_{wf}, no doubt associated with Zeeman coupling of the WF phase to the applied H [44], naturally leading to an associated transition in resistivity, and thus "metamagnetic MR." As is typical [43,44], the metamagnetic MR here is negative, indicating that ρ is lower in the WF phase than the AF phase. The effect is also essentially isotropic in Figs. 2(f) and 2(h), and small in magnitude compared to systems such as FeRh [43,44]. Lower MR at a field-driven AF to WF transition compared to an AF to F transition is intuitive, although a more quantitative understanding would obviously require a better appreciation of the origin of the WF state in NiS_2.

C. Magnetoresistance due to weak ferromagnetic switching, and exchange bias ($T < T_{wf}$)

1. Experimental findings

As shown in Figs. 1(d) and 1(h), cooling significantly below T_{wf} switches off the MR mechanism discussed in Sec. III B, instead inducing a distinctly different form of MR. Figure 3 illustrates this latter effect through the behaviors of $M(H)$ and MR(H) in the two H directions at a representative $T \approx 20$ K. Figures 3(a) and 3(d) show the expected $M(H)$ behavior at this T, where the soft WF component appears superimposed on a nonsaturating, essentially linear "background" due to the coexisting AF order [10,14,25,26]. The interesting finding here, however, is that the $M(H)$ behaviors with H//[111] and $\perp$[111] are distinctly different. Specifically, the H//[111] data in Fig. 3(a) (i.e., with H perpendicular to the surface) reveal clear anomalies at critical field magnitudes we label H^*, which are not present when $H\perp$[111] [Fig. 3(d)]. This field scale H^* is found at all $T < T_{wf}$ when H is applied //[111], as shown below. Most significantly, Figs. 3(c) and 3(f) show that the anomaly at H^* for H//[111] appears not only in $M(H)$, but also in MR(H), as a sharp decrease in ρ, i.e., negative MR commencing at H^*. This is underscored by the vertical dashed lines in Figs. 3(a)–3(c), which illustrate the abrupt coincident changes in $M(H)$ and MR(H) at $\pm H^*$. A similar phenomenon is visible at certain temperatures in the local MR data acquired on NiS_2 nanoflakes recently, where it reaches very large amplitudes, exceeding 1000% [40].

That the MR effects in Figs. 3(c) and 3(f) are clearly magnetically driven is highlighted by Figs. 3(b) and 3(e), which plot $-M^2_{wf}(H)$ for comparison to MR(H). This quantity is

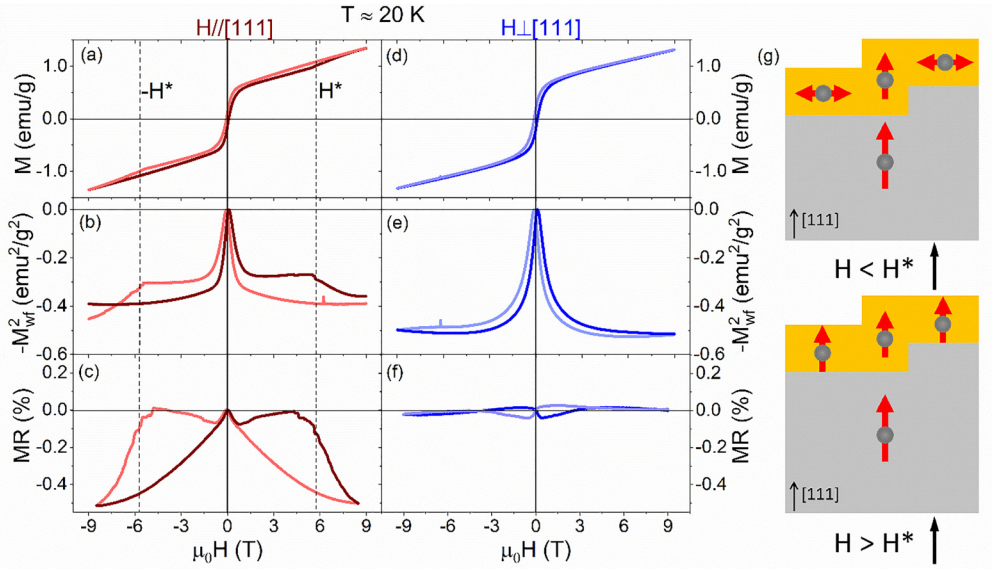

FIG. 3. Applied magnetic field (H) dependence of the magnetization [M, top panels (a),(d)], negative square of the weak ferromagnetic magnetization [$-M_{wf}^2$, middle panels (b),(e)], and percent magnetoresistance [MR, bottom panels (c),(f)] at temperature $T \approx 20$ K. [(a)–(c) were acquired at 15 K, (d)–(f) at 25 K]. Data are shown for H parallel to [111] (left, red) and perpendicular to [111] (right, blue). In the H//[111] case the reorientation field H^* is marked with the dashed vertical lines. In all cases, decreasing (negative direction) and increasing (positive direction) field sweeps are shown in lighter and darker shades, respectively. M_{wf} is isolated by removing the linear high-field background from the data in panels (a),(d). (g) Schematic of the proposed spin reorientation with H//[111]. Surface and bulk regions are shown in yellow and gray, respectively, and a single surface step (and thus two terraces) are shown; black arrows indicate the direction of H, parallel to [111].

determined by subtraction of the linear high-H component in Figs. 3(a) and 3(d) due to the AF order, thus isolating the WF magnetization, M_{wf}. The negative square of this quantity then provides an ideal comparison for MR(H) (see, e.g., [45]). The overall trends in H dependence in Figs. 3(b) and 3(e) indeed have clear similarities to those in Figs. 3(c) and 3(f), confirming the magnetic origin of this MR effect, and its link to the WF phase. Comparing Figs. 3(e) and 3(f), for example, it can be seen that the weak MR present for $H \perp [111]$ is analogous to the anisotropic magnetoresistance (AMR) observed in conductive ferromagnets [46]. On sweeping down from positive H (lighter lines), an MR peak occurs just past $H = 0$ at a small negative H, well correlated with $-H_c$ [the negative coercive field; see Fig. 3(d)]. A gradual decrease in ρ then occurs out to around -6 T [Fig. 3(f)], in good agreement with the WF magnetization behavior [Fig. 3(e)]. The reverse sweep to $+9$ T (darker lines) then follows the same behavior, but inverted, as expected. With H//[111], however, a similar AMR-type effect also arises [see the low-H correlations between Figs. 3(b) and 3(c)], but with the additional large drop in ρ (i.e., negative MR) at $\pm H^*$. Clearly, there thus exists some switching effect in the WF magnetization, *only for H//[111]*, which induces this larger, negative MR effect. We emphasize that whatever this switching effect is, it is anisotropic [see Figs. 3(a) and 3(d), and 3(c) and 3(f)], clearly related to the WF order, not the AF order [the magnetization associated with the latter is essentially isotropic, e.g., Figs. 2(a) and 2(c)], and must exist at the NiS_2 surface (as it is observed in these surface-dominated magnetotransport measurements).

Figure 4(a) shows the T dependence of H^*, obtained by warming above T_N and then cooling back to each T to take

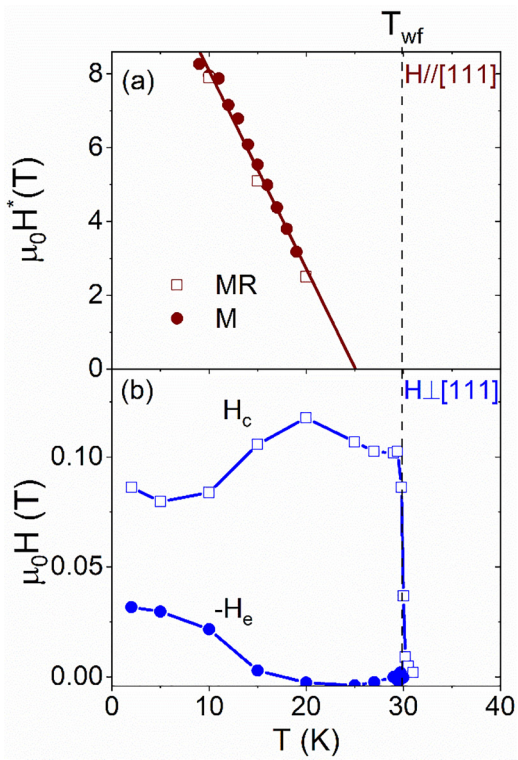

FIG. 4. Temperature (T) dependence of (a) the reorientation field H^* and (b) the coercive (H_c) and exchange-bias (H_e) fields. The weak ferromagnetic ordering temperature T_{wf} is marked. Necessarily, (a) is for H//[111] while (b) is for $H \perp [111]$. In (a), points are shown from both magnetoresistance (MR) and magnetization (M).

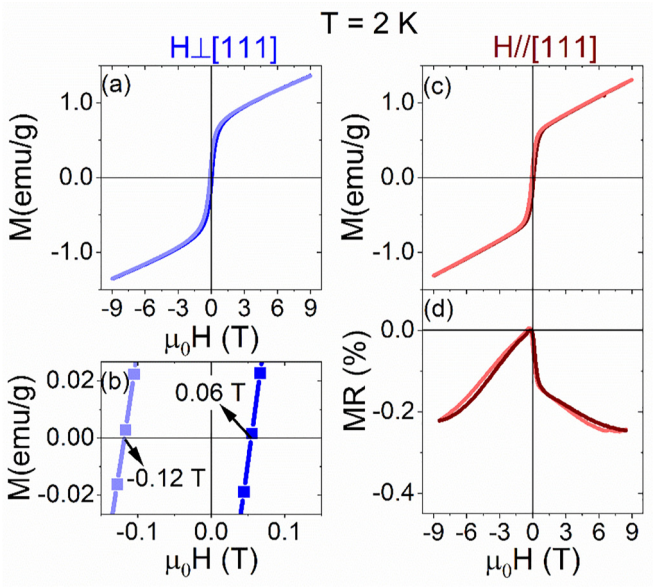

FIG. 5. Applied magnetic field (H) dependence of the magnetization M [top panels (a),(c)] and percent magnetoresistance MR (d) at temperature $T = 2$ K. Data are shown for H perpendicular to [111] (left, blue) and parallel to [111] (right, red). Panel (b) is a blowup of (a) illustrating the existence of exchange bias. In all cases, decreasing (negative direction) and increasing (positive direction) field sweeps are shown in lighter and darker shades, respectively.

isothermal $M(H)$ and MR(H) data. The measurements of H^* from MR and M (open and solid symbols, respectively) are reassuringly consistent, exhibiting a strikingly linear increase on cooling. At $T > 20$ K, H^* can no longer be easily identified as this field scale becomes sufficiently low that it begins to overlap with both the typical WF magnetization reversal at $\pm H_c$, and the H_{wf} as $T \to T_{wf}$. The linear extrapolation to $H^* = 0$ in Fig. 4(a) comes in at ∼26 K, however, close to T_{wf}, further confirming the link between H^* and the WF phase. Figure 4(a) thus demonstrates that as the system is cooled, and the magnetic order strengthens [Fig. 1(a)], the field required to trigger the switching event at H^* apparently increases linearly [Fig. 4(a)], eventually resulting in H^* exceeding the 9-T measurement window below ∼9 K. The MR behavior below this temperature is returned to below, later in this section.

Figures 5(a) and 5(b) further highlight that while no H^* occurs for $H \perp [111]$ (in the crystal plane), another interesting effect does arise. As can be seen in Fig. 5(a), but more clearly in the low-H close-up in Fig. 5(b), cooling to low-T (2 K in this case) induces clear exchange bias, only for $H \perp [111]$ (the equivalent $M(H)$ for $H//[111]$ is shown in Fig. 5(c) and reveals no exchange shift, even on close inspection). Interestingly, this exchange bias does not require deliberate cooling in a large field; it emerges even on cooling in a small remanent field, or after the initial application of a 9-T field at low T, i.e., "field poling" [47]. Explicitly, the left and right coercive points in Fig. 5(b) occur at −0.12 and 0.06 T, respectively, indicating a negative exchange-bias field, H_e (i.e., opposite to the remanent cooling field and low-T poling field), as is typical in exchange-biased systems [48,49]. The full T dependence of H_e and H_c is plotted in Fig. 4(b). H_c is seen to onset sharply on cooling below T_{wf}, consistent with the first-order nature of the AF to WF transition [10,26]. H_c then exhibits a clear change in behavior below ∼20 K, close to the point at which H_e emerges [20–25 K from Fig. 4(b)]. H_e then grows monotonically on cooling, in typical fashion for exchange-biased systems [48,49].

2. *Interpretation: Surface spin reorientation*

Considering Figs. 3–5 together, the picture that emerges is that a distinct magnetic switching phenomenon associated with the WF magnetization occurs below ∼20 K in NiS_2, only when H is applied along [111], perpendicular to the surface [Fig. 3(a)]. This switching phenomenon triggers a clear negative MR effect in surface transport [Fig. 3(c)]. Simultaneous with this, exchange bias develops when H is applied perpendicular to [111], i.e., parallel to the surface [Figs. 4(b), 5(a), and 5(b)]. Connecting these systematic findings with prior observations from local (micron-scale) MR measurements and magnetic microscopy on NiS_2 nanoflakes [40], we propose a consistent and unifying explanation for these effects. First, the exchange bias for $H \perp [111]$, in the crystal plane, likely simply reflects the interaction between WF and AF orders that would naturally be anticipated [48,49]. Figure 4(b) shows that this develops below an exchange-bias blocking temperature of 20–25 K, slightly below the T_{wf} ordering temperature, as is common in exchange-biased systems [48–50]. Explicitly, the AF order in NiS_2 is present at all T below $T_N \approx 39$ K, with the AF order parameter growing on cooling in second-order fashion. When the WF order then kicks in below T_{wf} (also modifying the overall AF order [24]) exchange bias develops due to coupling between the WF magnetization and the AF order parameter. The exact blocking temperature for such a phenomenon would be expected to deviate somewhat from T_{wf} (i.e., the lowest of the AF and F ordering points) depending on the magnitudes of the magnetocrystalline anisotropies involved [48–50]. The fact that these exchange-bias effects develop only for H in the crystal plane, i.e., in the (111) plane, may be consistent with prior neutron-diffraction-based measurements of the NiS_2 spin structure, which indicate AF alignment in alternating (111) sheets [24], i.e., a nominally uncompensated (111) surface.

Moving to the more interesting $H//[111]$ situation, we propose that the key factor to explain the intriguing WF switching events at H^* is the recent observation of high WF magnetization concentrated at step edges on NiS_2 surfaces [40]. That work used nitrogen-vacancy-center scanning microscopy to detect regions of the NiS_2 crystal surface with enhanced out-of-plane magnetic field, specifically below T_{wf} [40]. These regions were found to be correlated with step edges on the single-crystal surface, leading to the conclusion that out-of-plane WF magnetization is concentrated at surface defects such as step edges in NiS_2 [40]. It is interesting to note that this could be consistent with the recent claim that the magnetization in NiS_2 may be connected to domain walls associated with the complex AF order [14], as these walls could be pinned at such defects. Based on this, and the observations in Figs. 1, and 3–5, we propose the simple picture in Fig. 3(g) to explain the phenomena observed here.

As shown in Fig. 3(g), we split the NiS_2 into bulk (gray) and surface (yellow) regions, the latter carrying the transport

current at low T. Based in part on the recent magnetic microscopy results [40], we propose that the majority of the surface exhibits in-plane orientation of the WF magnetization, while surface steps have WF magnetization pinned out of plane. Assuming different magnitudes of magnetic anisotropy in the bulk and surface regions, which is easily justifiable, we then propose the situation in the top panel of Fig. 3(g). When small H is applied along [111] (perpendicular to the surface), the WF magnetization in the NiS_2 interior begins to align with H, more easily than the majority of the surface, i.e., the surface terraces. Consistent with Fig. 3(a), the WF magnetization thus increases in typical fashion with increasing H, dominated by the bulk. At H^*, however, we propose that a spin reorientation transition is triggered at the surface terraces, inducing an abrupt switch to the situation in the bottom panel of Fig. 3(g). The surface region then transitions from a situation where the transport current must flow between in-plane-oriented terraces through out-of-plane-oriented steps (top panel), to a situation where the current flows through uniform WF magnetization in the terraces *and* step edges, naturally explaining the onset of abrupt negative MR at H^* in Fig. 3(c). Explicitly, additional scattering at the interfaces between surface regions with differing WF spin alignment is extinguished at H^* due to the spin reorientation transition, decreasing the resistance. This simple picture also explains the abrupt increase in WF magnetization at H^* [Fig. 3(a)], the relatively small magnitude of this increase being due to the fact that it involves the surface, not the bulk. In addition, as T is increased and the magnetic anisotropies naturally decrease, one would then expect a decrease in the critical field for the spin reorientation transition, as illustrated in Fig. 4(a). When H is applied *perpendicular* to [111], however, in the plane of the crystal surface, the bulk WF magnetization simply aligns with H and the surface terraces obviously exhibit no reorientation to out of plane, and thus no H^* features arise in either M(H) or MR(H) [Figs. 3(d) and 3(f)]. This simple picture, based only on the prior observation of perpendicular WF magnetization at step edges [40] and different magnetic anisotropy in the surface and bulk, can thus qualitatively explain all of the key phenomena in Figs. 3–5.

3. *Lowest-T behavior: Field asymmetry*

Further elucidating some of the recent observations in local transport measurements on NiS_2 single-crystal nanoflakes [40], Figs. 5(c) and 5(d) illustrate what occurs in $M(H)$ and MR(H) for H//[111] at the lowest T probed (2 K). At this point, as noted in the above discussion of Fig. 4(a), the temperature has been lowered to the point that H^* exceeds the 9-T measurement window in this study. As shown in Fig. 5(c), there is thus no visible H^* in the $\pm 9-$ T $M(H)$ sweep. While it appears unusual at first sight, and in fact was highlighted as such in the recent nanoflake study [40], the resulting field-asymmetric MR(H) in Fig. 5(d) can also be qualitatively understood based on the above picture (Sec. III C 2). Specifically, the H sweep from $+9$ to -9 T displays the typical peak associated with the reversal of the WF magnetization at small negative H [as in Fig. 3(c)], but the sharp feature at H^* in Figs. 3(a)–3(c) is not hit because $|H^*| > 9$ T. A large fraction of the surface WF magnetization thus remains unswitched to the out-of-plane, [111], direction, meaning that the WF magnetization is not saturated and a minor loop is swept out on reversing H from -9 to $+9$ T on the return cycle. With respect to the schematic in Fig. 3(g), the situation in the bottom panel is thus not reached, i.e., the WF magnetization from the surface terraces is never reoriented to out of plane. The resulting MR(H) in Fig. 5(d) is therefore highly field asymmetric, bearing a striking resemblance to the MR curves reported at low T in the recent NiS_2 nanoflake study [40]. Note that the obvious asymmetry in MR(H) [Fig. 5(d)], while $M(H)$ shows no such behavior [Fig. 5(c)], is simply due to the former being surface dominated while the latter integrates over the surface and bulk, and is thus bulk dominated.

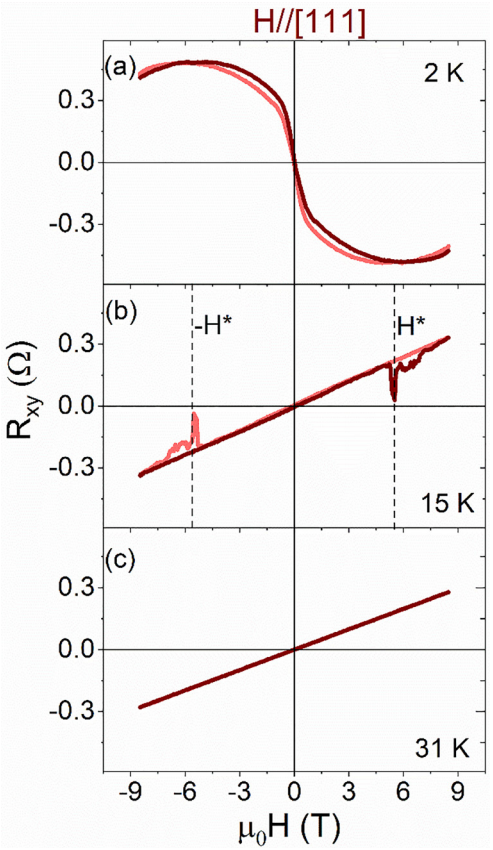

FIG. 6. Applied magnetic field (H) dependence of the transverse (Hall) resistance at (a) 2 K, (b) 15 K, and (c) 31 K, with H//[111]. In (b), the spin reorientation field H^* is shown by the vertical dashed lines. In all cases, decreasing (negative direction) and increasing (positive direction) field sweeps are shown in lighter and darker shades, respectively.

D. Corresponding Hall effects

Moving on from magnetoresistance, Fig. 6 shows that some of the exotic MR effects discussed above also manifest in interesting ways in the Hall channel. Shown here is the H dependence of the transverse (Hall) resistance R_{xy} at illustrative temperatures of 31, 15, and 2 K, obviously with H//[111] (perpendicular to the crystal plane and thus current flow). At 31 K [Fig. 6(c)], above T_{wf} and T_N, simple linear behavior is seen in $R_{xy}(H)$, with a positive slope and thus a positive Hall coefficient. This is consistent with our prior

observation of holelike transport in the surface state of NiS_2 single crystals [26]. While the Hall effect is far from straightforwardly interpreted in Mott insulators, this sign is consistent with FeS_2 surface transport [29–33], where the band bending at the surface is upward, resulting in the chemical potential moving toward the valence band edge [51], irrespective of the bulk doping (which can be *n* type [29–33,51,52] or *p* type [53] in single-crystal FeS_2). Intriguingly, at 15 K [Fig. 6(b)], below T_{wf}, the linear behavior in $R_{xy}(H)$ persists, but with clear additional features near $\pm H^*$ (marked by the dashed vertical lines). The irregular signatures in $R_{xy}(H)$ at these fields in fact bear a striking resemblance to the similarly chaotic behavior that is seen upon close inspection of MR(H) near $\pm H^*$ [see Fig. 3(c)], likely indicating some stochasticity in the exact switching field H^* across the NiS_2 surface. This is consistent with the above interpretation (Sec. III C 2) in terms of surface steps and terraces [Fig. 3(g)], which will obviously vary in their exact structure, and thus magnetic structure, from point to point on the surface.

Cooling well below T_{wf}, to 2 K, where the WF order fully develops, then leads to the behavior in Fig. 6(a), where, remarkably, $R_{xy}(H)$ exhibits a sizable, nonlinear, saturating component, superimposed on the linear positive component seen in Figs. 6(b) and 6(c). Given the clear presence of WF in this system, and the broad consistency of the data in Fig. 6(a) with the soft nature of the WF magnetization [see Fig. 5(c)], we ascribe this to an anomalous Hall effect associated with the WF order, which does not seem to have been previously detected in NiS_2. The anomalous Hall coefficient is apparently negative, i.e., opposite in sign to the ordinary Hall coefficient. Figure S2 in the Supplemental Material [42] thus inverts the Hall signal in Fig. 6(a), and subtracts the ordinary Hall contribution, to better isolate the anomalous Hall effect alone. A deeper understanding of this anomalous Hall effect in NiS_2 will likely require an improved understanding of the actual origin of the WF order. The high current general interest in anomalous Hall effects in AF systems [54] suggests that further work along these lines would not only be very worthwhile in terms of understanding NiS_2, but also on a more general level. We note that the T dependence here is of some interest, as the anomalous Hall signal develops only below $\sim$10 K, quite far beneath T_{wf}. As final comments on the 2 K data in Fig. 6(a), we point out that (i) no additional switching features due to the spin reorientation transition are present in $R_{xy}(H)$, due to H^* exceeding 9 T at this temperature; (ii) the exact form of $R_{xy}(H)$ in Fig 6(a) and $M(H)$ in Fig. 5(c) expectedly differ because $R_{xy}(H)$ is purely surface dominated; and (iii) $R_{xy}(H)$ exhibits none of the field asymmetry seen in MR(H) at this temperature [Fig. 5(d)]. The latter observation is presumably due to the fact that the anomalous Hall effect is sensitive only to the out-of-plane magnetization, unlike the MR, which is clearly impacted by the interfaces between in-plane and out-of-plane magnetized regions [see Fig. 3(g), top panel].

IV. SUMMARY AND CONCLUSIONS

A full study has been presented of the magnetotransport phenomena that emerge at low temperatures in NiS_2, deep in the surface transport regime, and below both the antiferromagnetic and weak ferromagnetic ordering temperatures. The onset of weak ferromagnetic order is found to have a particularly significant effect on transport, generating an anomaly in the temperature dependence of the resistivity and an isotropic negative magnetoresistance sharply peaked near the weak ferromagnetic ordering temperature. This has been explained in terms of metamagnetic magnetoresistance, i.e., the influence of a magnetic-field-induced antiferromagnetic to weak ferromagnetic transition on the resistivity. At lower temperatures, a larger, negative, anisotropic magnetoresistance then emerges. This occurs only for fields parallel to [111], perpendicular to the surface, due to a distinct switching event associated with the weak ferromagnetism. In light of exchange-bias effects in the in-plane direction, and recent observations of heightened weak ferromagnetism in the vicinity of steps on the NiS_2 surface [40], we consistently interpret these results in terms of a field-driven surface spin reorientation. At the lowest temperatures, the critical field for this transition eventually exceeds the 9-T measurement window, resulting in pronounced field asymmetry in the magnetoresistance sweeps, further demystifying recent observations in NiS_2 nanoflakes [40]. Finally, some of these phenomena also manifest in the Hall effect, in particular, generating a sizable anomalous Hall effect at the lowest temperatures, likely associated with the weak ferromagnetic order. These results substantially clarify the magnetotransport properties of this extensively studied model antiferromagnetic Mott insulator, yet further highlight the importance of surface transport in this system, and create a foundation to better understand the transitions from Mott insulator to metal with electron/hole doping and bandwidth control in the future.

ACKNOWLEDGMENTS

This work was supported primarily by the U.S. Department of Energy through the University of Minnesota Center for Quantum Materials under Grant No. DE-SC-0016371. S.E.-K. acknowledges Faculty Research Grants No. FRG20-M-S138 and No. FRG22-E-S93 from the American University of Sharjah. We are grateful for informative discussions with Angelo Di Bernardo.

[1] N. Mott, *Metal-Insulator Transitions*, 2nd ed. (Taylor & Francis, London, 1990).
[2] M. Imada, A. Fujimori, and Y. Tokura, Rev. Mod. Phys. **70**, 1039 (1998).
[3] P. A. Lee, N. Nagaosa, and X.-G. Wen, Rev. Mod. Phys. **78**, 17 (2006).
[4] H. S. Jarrett, W. H. Cloud, R. J. Bouchard, S. R. Butler, C. G. Frederick, and J. L. Gillson, Phys. Rev. Lett. **21**, 617 (1968).
[5] T. A. Bither, R. J. Bouchard, W. H. Cloud, P. C. Donohue, and W. J. Siemons, Inorg. Chem. **7**, 2208 (1968).
[6] S. Ogawa, S. Waki, and T. Teranishi, Int. J. Magn. **5**, 349 (1974).
[7] S. Ogawa, J. Appl. Phys. **50**, 2308 (1979).

[8] R. L. Kautz, M. S. Dresselhaus, D. Adler, and A. Linz, Phys. Rev. B **6**, 2078 (1972).

[9] T. Miyadai, K. Takizawa, H. Nagata, H. Ito, S. Miyahara, and K. Hirakawa, J. Phys. Soc. Jpn. **38**, 115 (1975).

[10] K. Kikuchi, J. Phys. Soc. Jpn. **47**, 484 (1979).

[11] M. Matsuura, Y. Endoh, H. Hiraka, K. Yamada, A. S. Mishchenko, N. Nagaosa, and I. V. Solovyev, Phys. Rev. B **68**, 094409 (2003).

[12] P. G. Niklowitz, P. L. Alireza, M. J. Steiner, G. G. Lonzarich, D. Braithwaite, G. Knebel, J. Flouquet, and J. A. Wilson, Phys. Rev. B **77**, 115135 (2008).

[13] Y. Feng, R. Jaramillo, A. Banerjee, J. M. Honig, and T. F. Rosenbaum, Phys. Rev. B **83**, 035106 (2011).

[14] T. Higo and S. Nakatsuji, J. Phys. Soc. Jpn. **84**, 053702 (2015).

[15] C. Clark and S. Friedemann, J. Magn. Magn. Mater. **400**, 56 (2016).

[16] A. K. Mabatah, E. J. Yoffa, P. C. Eklund, M. S. Dresselhaus, and D. Adler, Phys. Rev. Lett. **39**, 494 (1977).

[17] A. K. Mabatah, E. J. Yoffa, P. C. Eklund, M. S. Dresselhaus, and D. Adler, Phys. Rev. B **21**, 1676 (1980).

[18] P. Kwizera, A. K. Mabatah, M. S. Dresselhaus, and D. Adler, Phys. Rev. B **24**, 2972 (1981).

[19] A. Maignan, R. Daou, E. Guilmeau, D. Berthebaud, T. Barbier, O. Lebedev, and S. Hébert, Phys. Rev. Mater. **3**, 115401 (2019).

[20] F. Gautier, G. Krill, M. F. Lapierre, P. Panissod, C. Robert, G. Czjek, J. Fink, and H. Schmidt, Phys. Lett. A **53**, 31 (1975).

[21] P. Kwizera, M. S. Dresselhaus, and D. Adler, Phys. Rev. B **21**, 2328 (1980).

[22] Y. Sekine, H. Takahashi, N. Mori, T. Matsumoto, and T. Kosaka, Phys. B (Amsterdam) **237**, 148 (1997).

[23] J. M. Honig and J. Spalek, Chem. Mater. **10**, 2910 (1998).

[24] S. Yano, D. Louca, J. Yang, U. Chatterjee, D. E. Bugaris, D. Y. Chang, L. Peng, M. Grayson, and M. G. Kanatzidis, Phys. Rev. B **93**, 024409 (2016).

[25] T. Thio, J. W. Bennett, and T. R. Thurston, Phys. Rev. B **52**, 3555 (1995).

[26] S. El-Khatib, B. Voigt, B. Das, A. Stahl, W. Moore, M. Maiti, and C. Leighton, Phys. Rev. Mater. **5**, 115003 (2021).

[27] T. Thio and J. W. Bennett, Phys. Rev. B **50**, 10574 (1994).

[28] D. D. Sarma, S. R. Krishnakumar, E. Weschke, C. Schüßler-Langeheine, C. Mazumdar, L. Kilian, G. Kaindl, K. Mamiya, S.-I. Fujimori, A. Fujimori, and T. Miyadai, Phys. Rev. B **67**, 155112 (2003).

[29] M. Limpinsel, N. Farhi, N. Berry, J. Lindemuth, C. L. Perkins, Q. Lin, and M. Law, Energy Environ. Sci. **7**, 1974 (2014).

[30] D. Liang, M. Cabán-Acevedo, N. S. Kaiser, and S. Jin, Nano Lett. **14**, 6754 (2014).

[31] M. Cabán-Acevedo, N. S. Kaiser, C. R. English, D. Liang, B. J. Thompson, H. Chen, K. J. Czech, J. C. Wright, R. J. Hamers, and S. Jin, J. Am. Chem. Soc. **136**, 17163 (2014).

[32] J. Walter, X. Zhang, B. Voigt, R. Hool, M. Manno, F. Mork, E. S. Aydil, and C. Leighton, Phys. Rev. Mater. **1**, 065403 (2017).

[33] B. Voigt, W. Moore, M. Maiti, J. Walter, B. Das, M. Manno, C. Leighton, and E. S. Aydil, ACS Mater. Lett. **2**, 861 (2020).

[34] M. Z. Hasan and C. L. Kane, Rev. Mod. Phys. **82**, 3045 (2010).

[35] B. Yan and S.-C. Zhang, Rep. Prog. Phys. **75**, 096501 (2012).

[36] Y. Ando, J. Phys. Soc. Jpn. **82**, 102001 (2013).

[37] Y. Xu, L. Elcoro, Z.-D. Song, B. J. Wieder, M. G. Vergniory, N. Regnault, Y. Chen, C. Felser, and B. A. Bernevig, Nature (London) **586**, 702 (2020).

[38] E. Day-Roberts, R. M. Fernandes, and T. Birol, Phys. Rev. B **107**, 085150 (2023).

[39] N. Wu, R. F. Sabirianov, W. N. Mei, Y. B. Losovyj, N. Lozova, M. Manno, C. Leighton, and P. A. Dowben, J. Phys.: Condens. Matter **21**, 295501 (2009).

[40] R. Hartmann, M. Hogen, D. Lignon, A. K. C. Tan, M. Amado, S. El-Khatib, M. Egilmez, B. Das, C. Leighton, M. Atature, E. Scheer, and A. Di Bernardo, Nanoscale **15**, 10277 (2023).

[41] Explicitly, the data in Fig. 5(d) were not symmetrized. As discussed in the text, these data are highly field asymmetric, for reasons that are discussed in detail.

[42] See Supplemental Material at http://link.aps.org/supplemental/10.1103/PhysRevMaterials.7.104401 for the derivative data discussed in connection with Fig. 2 and the isolation of the anomalous Hall effect discussed in connection with Fig. 6.

[43] P. A. Algarabel, M. R. Ibarra, C. Marquina, A. del Moral, J. Galibert, M. Iqbal, and S. Askenazy, Appl. Phys. Lett. **66**, 3061 (1995).

[44] M. Sharma, H. M. Aarbogh, J.-U. Thiele, S. Maat, E. E. Fullerton, and C. Leighton, J. Appl. Phys. **109**, 083913 (2011).

[45] J. Wu, J. W. Lynn, C. J. Glinka, J. Burley, H. Zheng, J. F. Mitchell, and C. Leighton, Phys. Rev. Lett. **94**, 037201 (2005).

[46] T. R. McGuire and R. I. Potter, IEEE Trans. Magn. **11**, 1018 (1975).

[47] B. M. Wang, Y. Liu, P. Ren, B. Xia, K. B. Ruan, J. B. Yi, J. Ding, X. G. Li, and L. Wang, Phys. Rev. Lett. **106**, 077203 (2011).

[48] J. Nogues and I. K. Schuller, J. Magn. Magn. Mater. **192**, 203 (1999).

[49] A. E. Berkowitz and K. Takano, J. Magn. Magn. Mater. **200**, 552 (1999).

[50] H. Xi and R. M. White, J. Appl. Phys. **94**, 5850 (2003).

[51] A. Ennaoui, S. Fiechter, C. Pettenkofer, N. Alonso-Vante, K. Büker, M. Bronold, C. Höpfner, and H. Tributsch, Sol. Energy Mater. Sol. Cells **29**, 289 (1993).

[52] B. Voigt, W. Moore, M. Manno, J. Walter, J. D. Jeremiason, E. S. Aydil, and C. Leighton, ACS Appl. Mater. Interfaces **11**, 15552 (2019).

[53] B. Voigt, L. S. Valor, W. Moore, J. Jeremiason, J. Kakalios, E. S. Aydil, and C. Leighton, ACS Appl. Mater. Interfaces **15**, 28258 (2023).

[54] L. Smejkal, A. H. MacDonald, J. Sinova, S. Nakatsuji, and T. Jungwirth, Nat. Rev. Mater. **7**, 482 (2022).